Experimental investigation of waverider aerodynamic forces and shock waves in hypersonic slip regime in the wind tunnel MARHy

Viviana Lago, Noubel Hugo

HiSST: 2nd International Conference on
High-Speed Vehicle Science & Technology

11–15 September 2022, Bruges, Belgium

Experimental investigation of waverider aerodynamic forces and shock waves in hypersonic slip regime in the wind tunnel MARHy

Hugo Noubel [1], *Viviana Lago* [2], *Céline Baranger* [3]

Abstract

This paper presents an experimental investigation focused on aerodynamic forces and shock waves of a waverider. The study is carried out in the wind tunnel MARHy located at the ICARE laboratory of CNRS-Orleans. The facility can recreate the atmospheric re-entry flight of any vehicle in terms of viscous parameter and Knudsen number. The present work was carried out at hypersonic flow condition with a Mach number 20 and low density equivalent to 100 km of altitude. The model is a waverider optimized for optimal Lift to Drag ratio at Mach 10 and 50 km of altitude. The objective of this work is to analyse the behaviour of this waverider at high Mach number and altitude. The investigation of aerodynamic forces shows the waverider falls down for angles of attack higher than 15°. To confirm and explain this stall density inside the shock wave have been analysed from flow field a visualisation. This study shows a phenomenon of separation bubble which imply a constant pressure at the waverider surface. The bubble is observed thanks to luminosity intensity profiles and showing the displacement and increase of this bubble with the local rarefaction degree. As a consequence the shear layer can not reattach due to the separation bubble so the lift force decrease and the waverider falls down.

Keywords: *Mach 20.2 , Wind tunnel, Waverider, rarefied flows, Aerodynamic forces*

Introduction

The aerodynamic efficiency of a vehicle's flight is rated by the maximum of Lift-to-Drag (L/D) ratio of the forces acting on the vehicle. Waveriders are designed as the class of hypersonic vehicles that generate the highest L/D value compared to generic hypersonic designs. The characteristic of this type of vehicle is to generate a shock wave which remains attached under the leading edge to create a high L/D ratio and glide.

The first waverider concept appeared in 1959 with the work of Professor Terence Nonweiler [1] on folded delta wings which were named "Caret-wings". The design of waveriders was then improved with the work of M.L. Rasmussen [2] who developed a method for designing waveriders based on the shock created by a circular cone in a supersonic or hypersonic and inviscid flow fields. Waveriders are designed for a flight path point in terms of Mach number and flight altitude. Their geometry is therefore optimized for a specific flight condition, and outside of this configuration the flight skills of the waveriders will be degraded. Over decades many works were addressed to improve methods for calculating geometry waveriders for a wide Mach range of practical applications. Morphing waveriders have been proposed by Maxwell and all [3]. The concept focuses on morphing bottom surface providing on-design waverider aerodynamic performance across a wide range of Mach numbers [4]. All these strategies are developed with CFD models based on perfect fluid flow fields [5, 6].

This implies that viscous fluid effects are not integrated as a parameter of the numerical simulations.

[1] *CNRS, ICARE, UPR 3021, 1C avenue de la Recherche Scientifique, CS 500060, F-45071, Orléans, cedex 2 , France, hugo.noubel@cnrs-orleans.fr*

[2] *CNRS, ICARE, UPR 3021, 1C avenue de la Recherche Scientifique, CS 500060, F-45071, Orléans, cedex 2 , France, Viviana.lago@cnrs-orleans.fr*

[3] *CEA-CESTA, 15 avenue des Sablières, CS 60001, 33116 Le Barp Cedex, France, celine.baranger@cea.fr*

However, part of the waverider trajectory takes place at high altitude where the inviscid flow assumption is irrelevant. A realistic design should also consider viscous effects with constrained wall shear, weak and strong hypersonic viscous interaction, boundary layer displacement and high altitude slip flow effects. When slip effects become large, a viscous boundary layer results with a non-zero slip velocity condition at the wall, which increases viscous drag, thus decreasing the flight efficiency.

In the literature, there are few experimental results obtained under flow conditions in slip regime and or rarefied. Those that exist relate to works carried out with flat plates and delta wings [7, 8, 9, 10].

New experimental results are therefore useful and necessary to validate and possibly improve the numerical results that seek to optimize the design and the flight path of this type of vehicle. Few research on waverider shock waves in low density flows can be found in the literature. In 1986, Anderson [11, 12] included skin friction effects in the optimization process and proposed a new generation of waveriders named optimized viscous hypersonic waveriders.

The authors studied the behaviour of a waverider in supersonic flows in the slip regime. The waverider geometry studied is inspired by the design proposed by Rolim [13] and has been optimised for a flow at Mach 10 and an altitude of 50 km. Our first approach is to study the behaviour of this waverider outside the optimal conditions. A first step of the study has been carried out for supersonic Machs numers.

Experimental work was carried out in the MARHy supersonic/hypersonic rarefied wind tunnel. Three flow conditions were studied: Mach 2- 8 Pa, Mach 4 - 2.67 Pa and Mach 4 - 8 Pa giving viscous parameter values ($\sqrt{Re}/Mach$) of 13.91, 10.62, and 18.34 respectively indicating that the experimental flow conditions obey the slip regime. Our experimental work investigates the behaviour of the Lift-to-Drag ratio as a function of operating conditions and angle of attack [14]. Shock wave visualisations were analysed to establish a relationship between the evolution of lift and drag forces with shock wave angles for upper and lower shocks [15].

This experimental work presents the second step of our investigation focused on the study of the aerodynamic behaviour of the same waverider for hypersonic conditions at Mach 20.2 and a very rarefied flow regime as it corresponds to an altitude of 100 km. We also present measurements of drag and lift forces and an investigation of their behaviour based on detailed shock analysis.

1. Experimental condition

1.1. Waverider model

For this study, the investagated waverider is based on the work of Rolim [13]. The initial waverider is taking part of the bresilian waverider project 14-X. The waverider used is optimized thanks to the Rasmussen method which does not take into account viscous effects. This is one of the reason why the Rolim waverider is optimized for 50 km and Mach 10. In this study, the flow investigated is Mach 20 and the static pressure associated is $6.7.10^{-2}$ Pa which is typical to altitude of 90 kilometers. The objective is to alaysed the aerodynamic behaviour of the waverider when it flies at altitudes higher than the initial optimisation and at speed higher than the optimal. The waverider has already been investigated for Mach numbers ranged between Mach 2 and Mach 4 for pressures associated to altitudes between 50 km and 70 km. The objective of this study is to analyse an extreme case where the rarefaction degree of the flow is high and the speed is maximum during a re-entry phase.

As mentioned before, the waverider is based on the Rolim waverider. Dimensions have been scaled to fit with the flow core of the experimental conditions. The maximum of length possible is 100 mm to be sure to be inside the flow core and realised a maximum of angle of attack. The test model is 100 mm long, 35.7 mm wide and 6.6 mm high, Fig.1. The top surface named the extrados is slightly curved and the boottom part named the intrados is flat.

1.2. Wind tunnel description

To create the hyperonic rarefied flow, the wind tunnel MARHy is used. This wind tunnel have been built in 1961 at the 'Laboratoire d'Aerothermique' in Meudon. Previously named SR3, when the wind

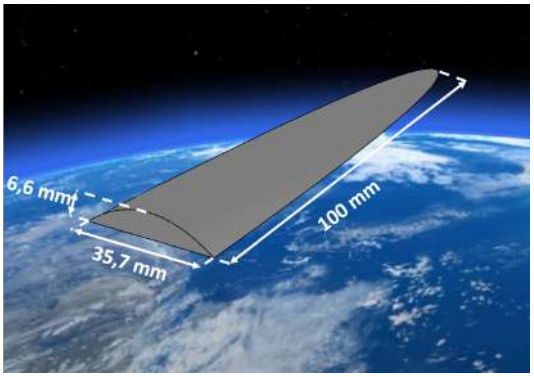

Fig 1. Waverider geometry

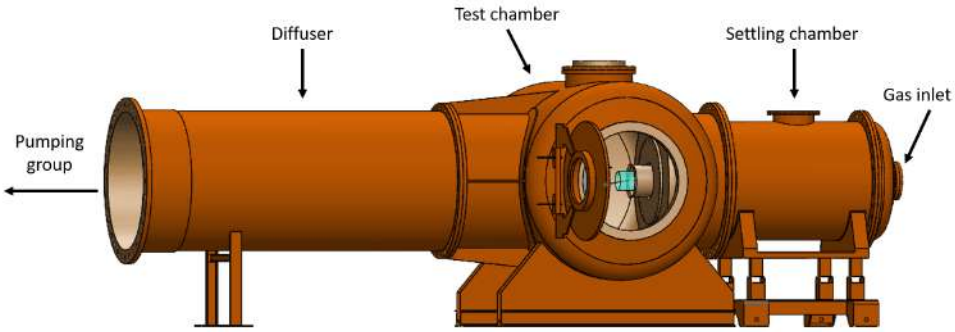

Fig 2. Wind tunnel MARHy

tunnel moved to the ICARE laboratory of Orleans after 40 years of working, the wind tunnel have been renamed MARHy (Mach Adaptable Rarefied Hypersonic), Fig.2.

The wind tunnel is composed of three part, the settling chamber, the test chamber and the pumping group.

The settling chamber is the beginning of the wind tunnel and it is the section where the gas is introduced and feed the contoured nozzle. To produce flows of different Mach numbers, the nozzle is changed and it allow to experiment subsonic, supersonic and hypersonic rarefied flows ranged between Mach number 0.8 and 20.2.

In this paper the hypersonic configuration is quite different than supersonic configurations. While for subsonic and supersonic rarefied flows, air is used, for hypersonic flows the used gas is nitrogen. Also, the hypersonic nozzle is different than the others because the gas, nitrogen, need to be heated to avoid freeze in the divergent section Nitrogen is introduced in a vessel where a graphite resistance will heat the nitrogen by Joule effect. After the carbon heater, nitrogen is compressed through the nozzle the throat and then expands through the divergent section of the nozzle. All components of the nozzle are cooled with a water circuit.

The test chamber is the next part of the wind tunnel. In this section, the test model is positioned closed to the exit nozzle to be sure to be inside the isentropic core. Instead of supersonic nozzles, the isentropic core for hypersonic nozzle is located close to the nozzle so the test model need to be positioned with accuracy to be sure to investigate the good flow conditions. The test chamber is a cylinder of 2 meters diameter and 3.5 meters long and positioned perpendicular to the flow. The large volume allows to use

several scientific devices inside the test chamber. In addition to intrusive instruments, optical cameras can be use thanks to two flanges equipped with quartz and fluorine optical windows.

Then the final part of the wind tunnel, the pumping unit Fig.3, which components have been entirely renewed during the transit between Meudon and Orleans. 2 primary pumps, 2 intermediary pumps and 12 root pumps compose the pumping unit. The association of 16 pumps allow to work without interruption for several hours. A diffuser through a butterfly valve connects the pumping unit and the testing chamber, which control the static pressure inside the testing chamber.

Fig 3. Wind tunnel MARHy pumping group

1.3. Operating condition

As presented before, different flow configuration can be experimented in the wind tunnel MARHy. In this study the hypersonic contoured nozzle Mach 20.2 - 0.068 Pa is used. This nozzle operates with nitrogen which is heated when it will cross a graphite heater. This heater is supplied with an electric generator at high intensity. The gas is warm at 827°C but the gas in the testing chamber is only 13.32 K.

Table 1. Flow conditions of the Mach 20.2 - 0.068 Pa nozzle

Stagnation conditions		**Free-stream conditions**	
gas	Nitrogen	gas	Nitrogen
P_o (Pa)	350000	P_∞ (Pa)	0.068
Te_o (K)	1100	Te_∞ (K)	13.32
ρ_o (kg.m^{-3})	1.07	ρ_∞ (kg.m^{-3})	1.73.10^{-5}
		μ_∞ (Pa.s)	9.12.10^{-7}
		U_∞ (m.s^{-1})	1502.14
		Re_∞ (m^{-1})	28480
		Ma_∞	20.2
		λ_∞ (m)	1.05.10^{-3}

2. Experimental description

In this study, two different experiments were carried out: first the study of aerodynamic forces by means a home-made aerodynamic sting balance and secondly the visualization of shock waves using the glow discharge technic.

2.1. Aerodynamic sting balance

The aerodynamic sting balance used to measure waverider aerodynamic force have been designed at the ICARE laboratory by Hugo Noubel [14], Fig.4. The principle of intern balance and more precisely

sting balance have been preferred to extern balance because intrusive devices can be used inside MARHy wiind tunnel and it offers more accuracy.

The sting balance is a two-axis balance which can measure only two forces: drag and lift. The balance has two separated modulus, one to measure the drag force and the second one to measure lift. Both modulus are composed by lamellae equipped with semiconductor strain gages. There are four strain gages on each modulus to compose a Winston bridge to improve the quality of measures and reduce thermal effects.

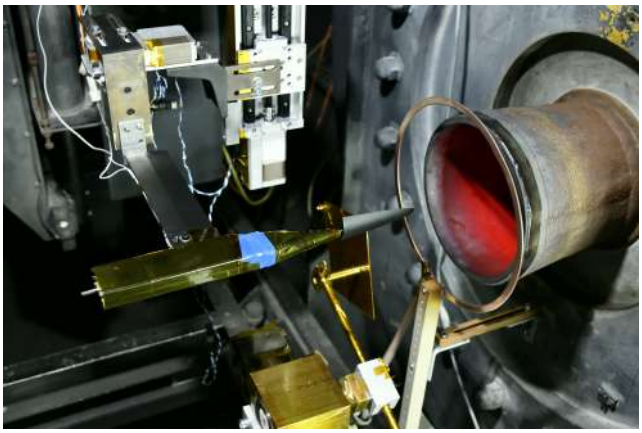

Fig 4. Sting balance positionned in the wind tunnel MARHy

The sting balance is positioned horizontally in the wind tunnel in order to impose an angle of attack on the waverider without being affected by the force of gravity and thus not being impacted by a change in the position of the model's centre of gravity. For each angle of attack, the aerodynamic forces must be corrected using trigonometric referential change formulae. For each angle of attack, the waverider is centrered in the flow core to keep the same free stream condition. When the angle of attack is too high and the free stream pressure too far from the optimal conditions the angle of attack is not studied. For this reason, the maximal angle of attack investigated for the hypersonic nozzle Mach 20.2 0.068 Pa is 20°.

Thanks to semi-conductor strain gages, this balance as a high accuracy. For each angle of attack, the measurements were carried out several times to ensure repeatability and to determine a mean value with a standard deviation. With the hypersonic nozzle forces, the minimal standard deviation between forces is 0.18 mN obtained for zero degree angle of attack.

2.2. Glow discharge

Different technics are usually applied to visualize shock waves arround a test model. These technics depend on the density of the flow. For example the PIV or Schlieren technics are not relevant for the present case because the density inside the test chamber is too low. To give an example, Settles [16] estimates the Schlieren technic appliable for density up to 1% of the atmospheriic density, i.e. 1.20.10^{-2} kg/m^3 and in the investigation flow density is about 1.73.10^{-5} kg/m^3. To fix the problematic of low density, the solution is to ionise the flow thanks to an electron beam or glow discharge.

For this investigation, the technic used is the glow discharge as it was already used in many supersonic flows configuration. giving good results n s As the Fig.5 shows it, the color of the ionized flow is pink. The Spectroscopic analysis of the ligth emitted by the the glow dishcarge showed the presence of only emissions from the 1^{st} negative system (N_2^+) at 391.4 nm and the 2^{nd} positive system (N_2) with a wavelength of 337 nm.

As described in the article of Noubel and coumar thesis [15, 17], the intensity of the glow discharge can be associated to the molecular concentration. The measured light intensity is correlated to density

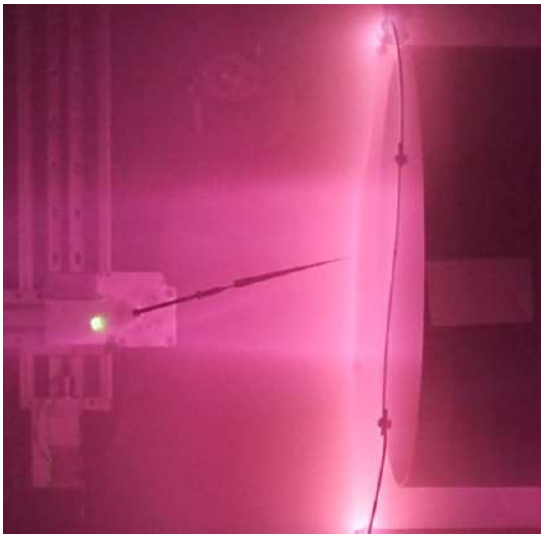

Fig 5. Glow discharge visualization

of the flow and so any variations of ligth intensity can be associated to variation of density and thus variation of pressure.

To visualize shock wave, the waverider is positioned at the center of the flow core, the glow discharge switch on and an image is record. Then the waverider is removed, the glow discharge still switches on and then a new image is recorded. This second image is a background which divided to the model/flow field image gives a better detection of the shock wave as the Fig.6 show it. For this study, glow discharge is obtained with the copper ring biased negatively with a voltage of -2 kV for an intensity of 7 mA.

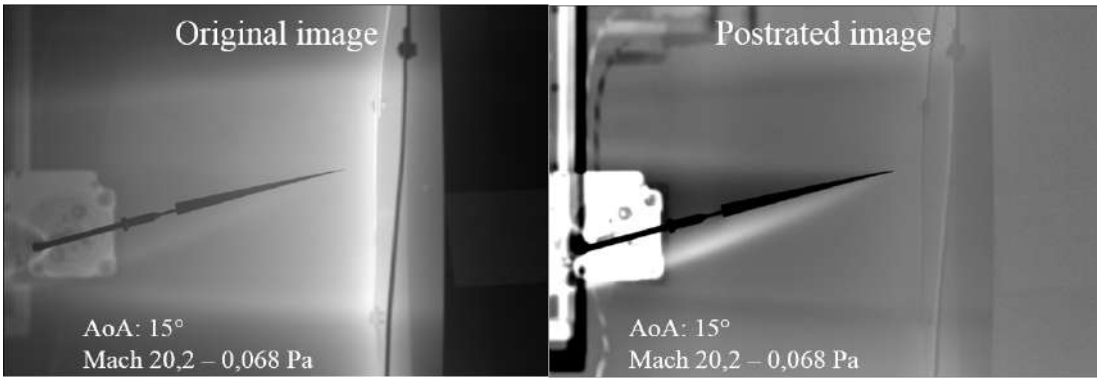

Fig 6. Original and postraited images

For the aerodynamic forces study, angles of attack investigated are ranged between 0° and 20°. The reason to not test angles of attack higher is due to experimental constraints in particular regarding the pressure inside the test section, which must remain close to the optimal value. One of the main reasons of the increase of pressure is due to the sting balance, which is too big for the flow. For the glow discharge study, the device is smaller than the sting balance and so the angle of attack 25° could be investigated in addition to the others.

3. Results

3.1. Aerodynamic forces

Aerodynamic forces have been measured for different angles of attack. Results are summarized on the Fig.7. Two curves are plotted representing the drag force in orange and the lift force in green. Both curves have different behave, the drag force is fitted with a quadratic curve with a minimum near 0°. For the lift force the trend curve is linear for angles of attack lower than 15° which is similar to investigations in supersonic rarefied flows presented by Noubel [14].

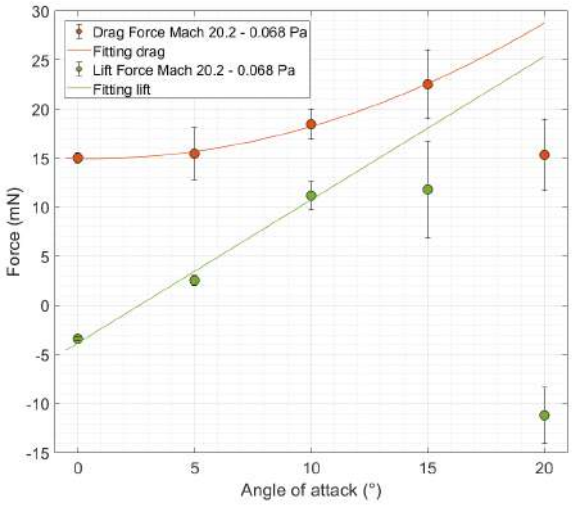

Fig 7. Drag and Lift forces measured for different angles of attack

In this study with hypersonic flow conditions, the force trends are similar to those determined in rarefied supersonic flow, but for angles of attack less than 15°. For angles of attack higher, both curves are falling down which is a new observation compared to previous studies.

The lift force curve can be divided in three parts. The first one is a linear increase between 0° and 10°, then the curve seems constant and finally after 15° the curve is drastically decreasing. This trend is similar to a phenomenon well known in the aeronautic which is the stall. The stall in aeronautic is a boundary layer separation which creates a drastic decrease of the lift force. The stall depends on the angle of attack, the wing shape and the flow conditions. Comparing lift curves during a stall [18] with the trends obtained here it seems that for angles of attack greater than 15° a stall is observed. An instability can be observed on lift force 15° point thanks to the big the standard deviation, obtained with the repetition of several measures.

One of the major indications of this aerodynamic forces study is on the angle of attack to be adopted during flight. Regardless of the values the Lift-to-Drag ratio we can say that during a hypersonic flight, if the pressure is too low around the waverider there is a risk of stalling and it can compromise the mission. The waverider studied does not have booster to correct its trajectory so if it reaches the stall angle it could have drastic impact on the trajectory. This study is important because it shows for the first time experimentally that a stall can be reached if a non-optimized waverider reach hypersonic speeds in rarefied flow. If the stall is reached, the waverider need to reduce its angle of attack to increase its speed and try to recover positive lift force.

If we interest on the Lift to Drag ratio we can see the curve increase and reach a maximal value at 10°. This angle characterizes the optimal angle for the waverider for this flow conditions. For an angle of ten degree, the waverider can flight on the highest distance possible and here for each vertical kilometre lose at these flow conditions, the waverider glide over 610 meters. These data show the waverider has poor aerodynamic performances because the Lift to Drag ratio is less than 1. The main reason of

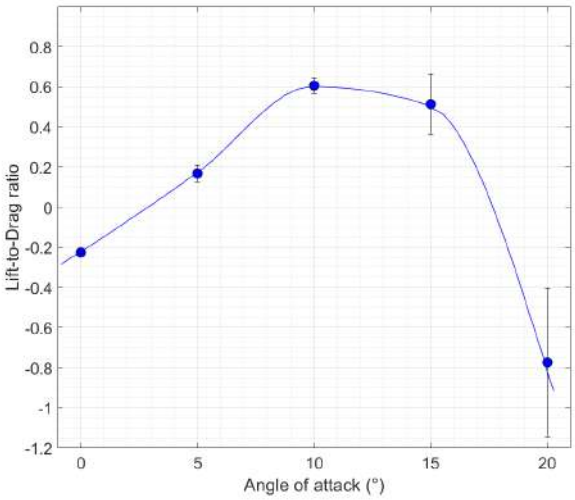

Fig 8. Lift-to-Drag ratio

these performances is due to the geometry, which is not optimized for these flow conditions. Indeed the boundary layer is not considered by the Rasmussen geometries design, but for this rarefied flow condition, the boundary layer is thick. Therefore, to improve aerodynamic performances the geometry need to be adapt to be able improve glide in hypersonic rarefied flows. On the Fig.8 the instability due to the stall can be observed thanks to the standard deviation and values which decrease after 15° as the a aerodynamic forces presented before.

3.2. Shock waves study

To confirm the stall determined from the analysis of aerodynamic forces, the shock wave on the extrados of the waverider is studied. In aeronautic when a stall is reached, a turbulent flow is observed on the extrados of the wing which leading to a decrease of lift. The goal of this section is to understand what the reason of the stall for a waverider is in hypersonic rarefied flow.

When the background is removed from the original iCCD image, the shock wave is better visible. Then, it is possible to determine the shock wave angle of the extrados and intrados but here the most important thing is what happen inside the extrados shock wave. As it is explained in previous subsection, the stall is a boundary layer separation and in the continuum regime, a vortex can be observed. If we refer to the Fig.6 there is no wortex visible on the original picture or on the prostrated image. The only way to observe a variation inside the extrados shock wave is to plot luminosity intensity profiles perpendicular to the upper surface. This method allows characterizing the variation of density inside the shock wave because luminosity intensity variations and density variations are related as explained in the section 'Glow discharge'.

Luminosity profiles are plotted along a straight line, which start at the end of the waverider surface and cross all the shock wave. As it is presented on the Fig.9, five profiles are plotted to have the evolution of the luminosity along the surface. This analysis is repeated for all the angles of attack. The profile at the waverider nose is not considered because we know there is an attached shock wave and the variations at the nose will not give any information on the variation of the pressure inside the shock, as it can be the case for the other profiles. So if the Fig.9 is considered, there are five profiles, starting by the left, named: profile 100 mm, profile 80 mm, profile 60 mm, profile 40 mm and finally profile 20 mm which is the closer profile to the nose.

For each profile a curve is obtained and give information on the shock density behaves. The Fig.10 presents the different regions of the shock. There are four regions in the graph, which describe the shock wave. The x-axis represents the length of the profile so at 0 mm it is associated to the waverider

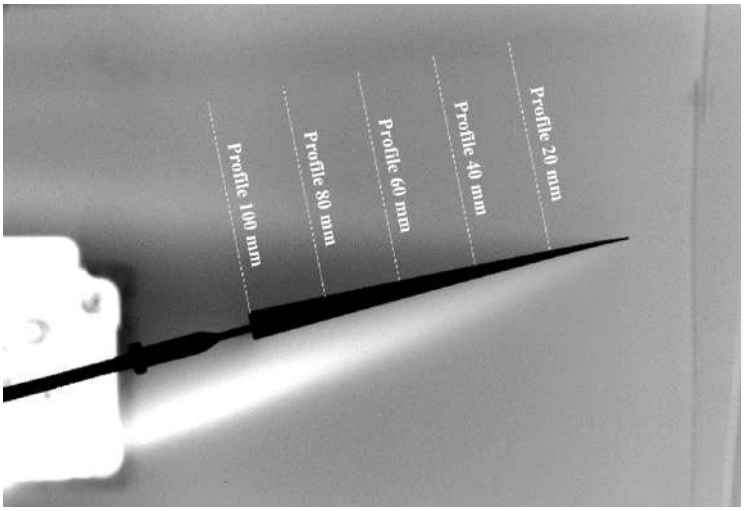

Fig 9. Waverider and profiles

surface.

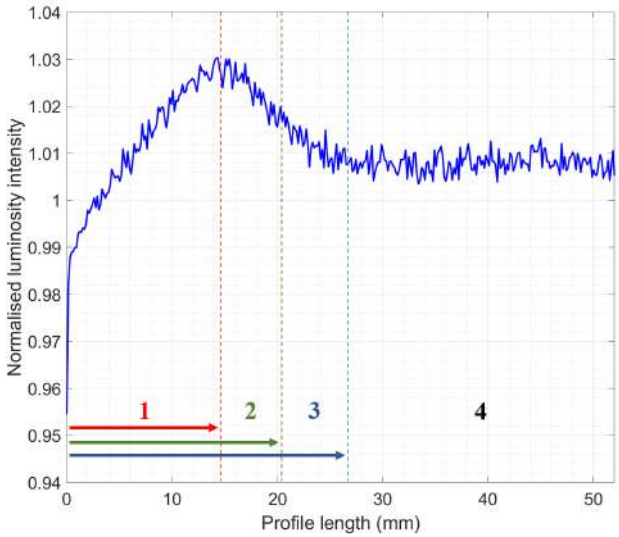

Fig 10. composition of the shock wave on a luminosity intensity profile

The first region is the boundary layer marked by the number one in red. It is characterised by an increase of the luminosity intensity and the distance between the wave rider surface (x = 0 mm) and the maximum of the luminosity intensity is considered as the boundary layer thickness. The more a flow is rarefied and the more the boundary layer will be thick. In continuum regime, for supersonic flows this region is extremely thin nevertheless it can be visible for hypersonic flows.

The second regioon of the curve is a decrease of the luminosity intensity. This decrease describes a curve and the inflection point of this curve, associated to the green dot line, is the middle shock [19]. The distance between the waverider surface (x = 0 mm) and the green dot line is the thickness of the shock.

The third region represented in blue is the transition between the decrease and the constant region of

the luminosity intensity. This region delimits the foot shock. After the foot shock, the curve is constant because the profile describes what happen outside the shock wave. Outside the shock wave the density is constant that is the reason why the luminosity intensity profile does not vary.

After considering a classical profile we will analyse all the profiles for all angles of attack to identify if anything can explain the stall observed for the aerodynamic forces studied Fig.7. Fig.11, presents the totally graph fo the profiles along the waverider for angles of attck up to 25 °. the x-axis is the axis length in mm from 0 mm to 60 mm and the y-axis is the normalized luminosity intensity. For each profiles the luminosity intensity is divided by the luminosity intensity outside the shock wave to compare all values to free stream conditions. Fig.11 allowed to detect any 'anormal' behaviour.

First of all, for angles of attack of 0° and 5° density profiles of shocks waves seems 'normal' because all the region of the shock (boundary layer, middle shock and foot shock) are well visible. For the angle of attack 5° the shock wave is thicker than the angle of attack of 0° because the local rarefaction degree above the extrados due to the angle of attack is bigger for 5°. The increase of shock wave thickness is due to a boundary layer thicker which is characteristic on profiles with the maximum of luminosity intensity reached for highest values of profile length.

For the case of the angle of attack 10° we can note that profiles are more horizontal and different region the shock wave density profiles are more difficult to be identified. This could be interpreted as a diffused shock. Nevertheless, profiles seems to be similar to those obtained for 5°.

Then for higher angles of attck some differences can be pointed that can explaine the measured variations of aerodynamic forces.

For the angle of attack 15°, the slope of the profile 100 mm is not linear as the previous profiles at 100 mm. The variation of density inside the shock wave does not increase normally and a flat region appear that can explain forces instabilities observed at 15°. This change of slope is more visible for the angle of attack 20°. The penultimate line shows a profile at 100 mm with a flat region and then an increase of luminosity intensity. The situation observed for the profile 100 mm at 15° is visible for the profile 80 mm at 20°. The flat region seems to propagate along the waverider extrados surface. This hypothesis is confirmed with the last line and the angle of attack of 25°. On this line the Profile 40 mm is similar to the profile 80 mm at 20° and the profile 100 mm at 15°. Then for the three other profiles of this line, each one starts with a flat region but the longest is near the waverider base. The profile at 100 mm of 25° start with a negative slope followed with a flat region and finally a positive slope. It shows an important variation of density inside the shock wave when local rarefaction degree is important.

In conclusion, to this shock wave analysis, when the angle of attack increases, the density inside the shock varies. For high angles of attack, the density near the surface is low and remains constant over a distance. This distance increases with the angle of attack and the phenomenon propagates along the waverider surface. For 15° angle of attack it is only located at the waverider base and then for 25° angle of attack the phenomenon is clearly visible at 40 mm of the waverider nose.

3.3. Discussion

With the two previous studies, aerodynamic forces and shock waves, we can state there is a correlation between them. Indeed the stall observed in the aerodynamic force begin for angles higher than 15°. At the same time, the shock wave investigation showed a variation of the density inside the shock wave, which can explain the stall.

The Fig.12 recap all the profiles plotted for each angle of attack. In light blue there is the profile at 20 mm, in orange the profile at 40 mm, in purple profile at 60 mm, in green profile at 80 mm and in dark blue the profile at 100 mm.

For angles of attack ranged between 0° and 10° the lift-to-drag ratio increases and aerodynamic forces follow the general trend: linear for the lift and quadratic for the drag. This behaviour is 'normal' as those of shock wave profiles e as explained in the Fig.10.

Then for the angle of attack 15° an instability was observed on aerodynamic forces which correspond to the first apparition of a flat region on shock wave profiles. Indeed the profile of 100 mm at 15° has a

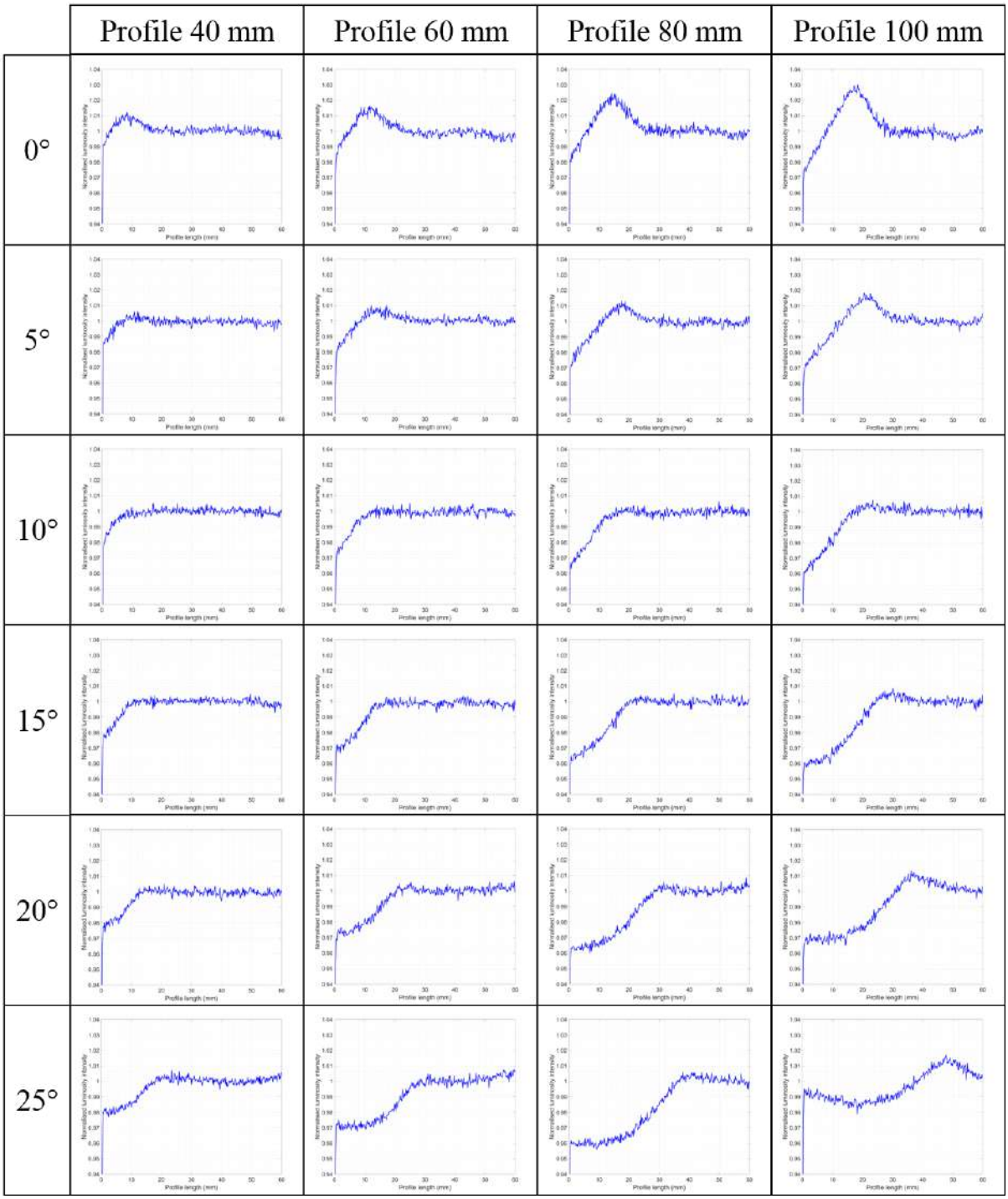

Fig 11. Detailed luminosity profiles plotted for each angle of attack

flat region near the surface which can be interpreted as a constant density value over 8 mm above the surface.

For the angle of attack of 20° the lift force and the Lift-to-Drag ratio decreases drastically. In this case, shock wave profiles present the flat region on the profile at 100 mm moreover the profile at 80 mm also presents a little flat region. All the profiles are normalised by the luminosity intensity outside the

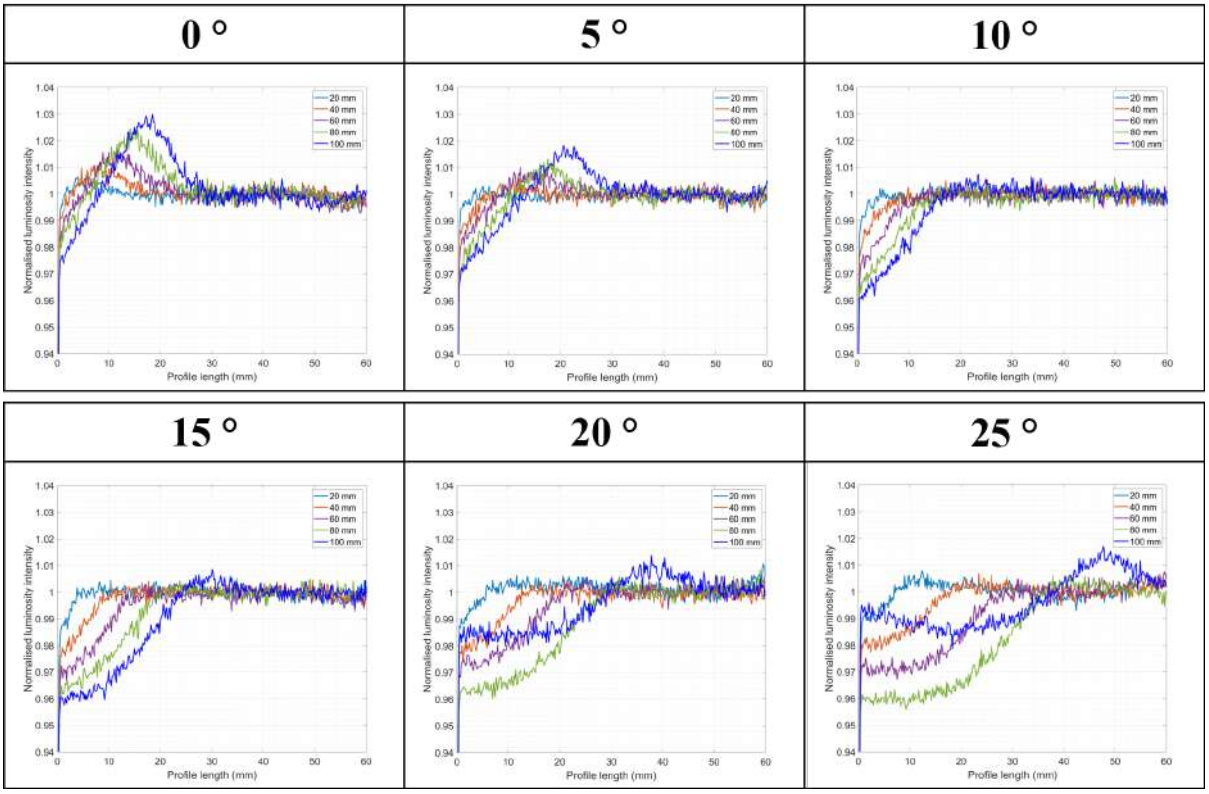

Fig 12. Luminosity intensity profiles regroup by angles of attack

shock wave corresponding to the free stream pressure. If the begining of the 100 mm profile of 20° is considered, it can be noted at the waverider surface the density is higher than density of profile 80 mm which is not observed for previous angles of attack. This observation means that the pressure on the waverider base increases so the increase of pressure creating a force toward the waverider surface. This pressure can explain why the waverider is falling down and have a negative lift force for 20°. This interpretation can be confirmed with results obtained with an angle of attack of 25° where the profile 100 mm as a surface density really high compared with the other cases and so we can suppose the lift force will still be negative. It is supposed the air stuck under the intrados move to the extrados and increase of pressure. Maxwell has already mentioned observation of flow recirculation [3]. The increase of pressure on the profile at 100 mm for all angles of attack is represented by the Fig.13. A complementary study will be necessary to measure the wall pressure to confirm a possible recirculation effect.

In 1972, Allegre and all made a study on delta wings for a flow at Mach 8 and a Reynolds number of 2200/cm. Flows conditions have lower speed and higher Re number than the present study. In their investigation, they determined aerodynamic forces and wall pressure for different angles of attack (between -20° and 20°). This study showed a stability on aerodynamic forces for all angles of attack and this stability is founded in the wall pressure results. The wall pressure for a same profile decrease and converge to a single value. It is not the case of our study where aerodynamic forces are not stable and the wall pressure seems to increase for 20° and 25° compared to the other angles. If there is no stall the lowest wall pressure for the profile 100 mm will be the same that for 25° and not 15°. The Allegre work seems to favour the hypothesis that the flat region that appears on the density profiles are indications of the creation of a phenomenon that distorts the density within the extrados shock wave.

Flat region on profiles are visible for three angles of attacks and seems to propagate in direction of the

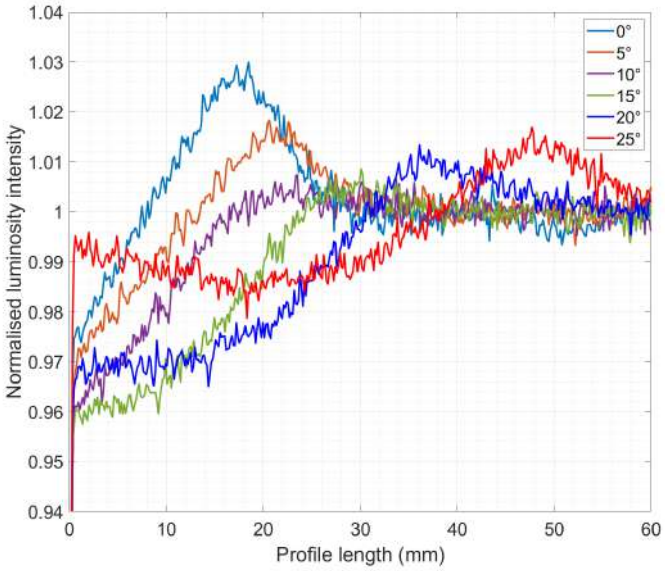

Fig 13. Luminosity intensity profile 100 mm for all angles of attack

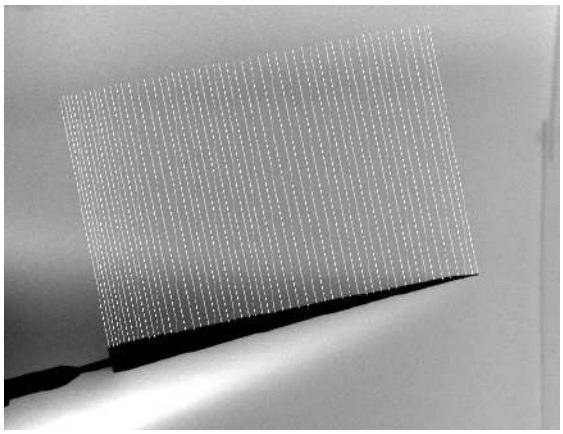

Fig 14. 3D mapping zone above the waverider

waverider nose when the angle of attack increases. To understand the origin of these flat regions, a 3D mapping of the variation of density above the extrados have been plotted. The Fig.14 represent the 3D mapping of four angles of attack. The blue region is the waverider surface and the region in dark red as a mountain represents the shock wave.

We can observe the emergence of a zone with a lower luminosity intensity (in green) for the angles of attack 15°, 20° and 25° and near the surface of the waverider. This zone seems to increase in size and move to the waverider nose, when angle of attack increases corresponding to the flat region of the density profiles. This zone seems round and it probably correspond to a separation bubble. Gaster [20] describes this phenomenon in 1966 in the domain of stall. This phenomenon appears in laminar conditions, and create a shallow region of reverse flow at the surface of an airfoil. The fluid in the forward region of the bubble is static which create a constant pressure region. This specificity can explain flat regions observed in the density profiles so it confirm the origin of stall. In his paper, Gaster precise that if the shear layer fails to reattach, the lift force fall. It is named the thin airfoil nose stall. This last point confirms that a variation of density in the extrados initiate the stall and the fall of

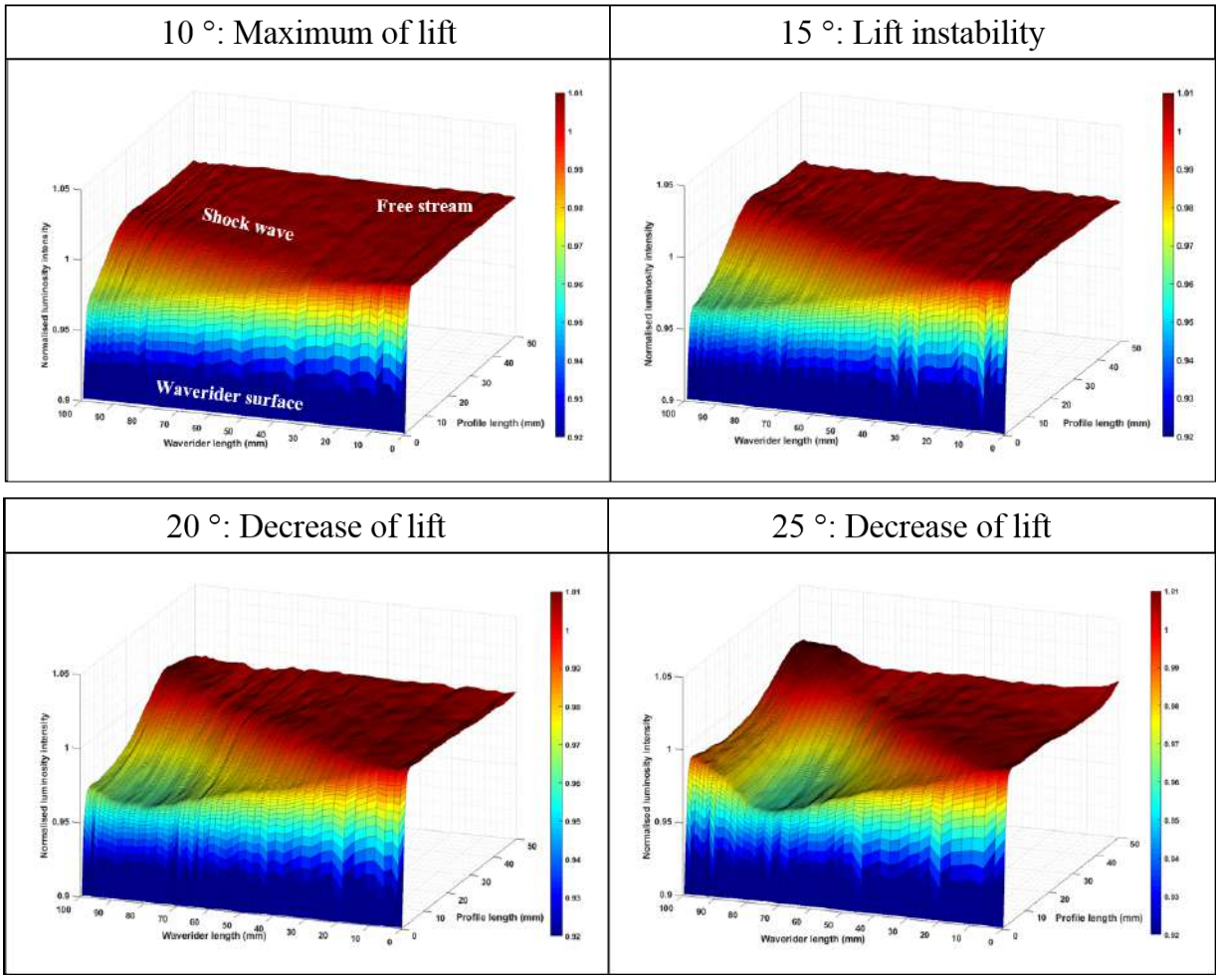

Fig 15. 3D mapping of the luminosity intensity to visualise the separation bubble

lift.

In conclusion, aerodynamic forces and shock waves are related because the creation of a separation bubble due to the low rarefaction degree, high angle of attack and flow conditions will change the density inside the shock wave. The density will be constant in the bubble and will imply a fall of the lift force and so a stall. The objective, if this situation appear, will be to reduce the angle of attack to reattached the shear layer and restoring lift and good aerodynamic performances.

Conclusion

The goal of this investigation was to determine aerodynamic forces of a waverider in slip regime at Mach 20.2. The waverider is based on the Rolim studies and it is designed thanks to the Rasmussen method. Aerodynamic forces are measured with an aerodynamic sting balance for angles of attack from 0° to 20°. This investigation shows that angles greater than 15° instabilities in the lift force appears. The lift force at 20° is negative so the waverider falls down. To understand the reason of the stall, a complementary study was realized to investigate and analyse the variation of pressure inside shock waves. The technic used is the glow discharge and the extrados shock wave is analysed because in case of stall, instabilities appear in this region. The shock wave study revealed that after 15° angle of attack the pressure remains constant near the waverider surface. This zone of constant pressure increase with the angle of attack and move to the waverider nose. This phenomenon is a separation bubble which appears between the surface and the boundary layer. Thanks to 3D mapping it have been concluded

the reason of the stall is due to this bubble which not allow the boundary layer to reattach and so create a fall of lift. To avoid the lift fall, the waverider need to reduce its angle of attack to remove the bubble. An other solution is to design a new waverider because a hypothesis of flow recirculation from the the bottom to the top can be made. The new waverider need to avoid recirculation and complementary studies will be realised. The objective is to mesure wall pressure and confirm the separation bubble and try to understand if there is a flow recirculation.

Acknowledgments

This work is fully financed by the Agence Nationale de la Recherche for the project APHYRA (APHYRA-19-ASTR-0014-01). PhD is supported by the French National Research Agency (ANR) as part of the Programme d'Investissements d'Avenir (LabEx CAPRYSSES; Grant No ANR-11-LABX-0006-01).

References

[1] T. Nonweiler, Aerodynamic problems of manned space vehicles, The Aeronautical Journal 63 (585) (1959) 521–528.

[2] M. L. Rasmussen, Waverider configurations derived from inclined circular and elliptic cones, Journal of Spacecraft and Rockets 17 (6) (1980) 537–545.

[3] J. R. Maxwell, Morphing waveriders for atmospheric entry, Ph.D. thesis, University of Maryland, College Park (2019).

[4] A. A. Phoenix, J. R. Maxwell, R. E. Rogers, Mach 5–3.5 morphing waverider accuracy and aerodynamic performance evaluation, Journal of Aircraft 56 (5) (2019) 2047–2061.

[5] J. Liu, F. Ding, W. Huang, L. Jin, Novel approach for designing a hypersonic gliding–cruising dual waverider vehicle, Acta Astronautica 102 (2014) 81–88.

[6] Y. Jianglong, D. Xiwang, L. Qingdong, R. Zhang, L. Jinhu, Cooperative guidance strategy for multiple hypersonic gliding vehicles system, Chinese Journal of Aeronautics 33 (3) (2020) 990–1005.

[7] S. Coumar, V. Lago, Influence of mach number and static pressure on plasma flow control of supersonic and rarefied flows around a sharp flat plate, Experiments in Fluids 58 (6) (2017) 1–16.

[8] J. Allègre, C. Bisch, Angle of attack and leading edge effects on the flow about a flat plate at mach number 18., AIAA Journal 6 (5) (1968) 848–852.

[9] J. Allegre, D. Lartigue, M.-F. Scibilia, Rarefied hypersonic flow characteristics of delta wings and trailing edge spoilers, AIAA Journal 10 (7) (1972) 900–905.

[10] J. Lengrand, J. Allegre, A. Chpoun, M. Raffin, Rarefied hypersonic flow over a sharp flat plate: numerical and experimental results, Progress in astronautics and aeronautics 160 (1994) 276–276.

[11] D. Capriotti, Viscous optimized hypersonic waveriders, in: 25th AIAA Aerospace Sciences Meeting, 1987, p. 272.

[12] J. Anderson Jr, K. Bowcutt, D. Capriotti, Viscous optimized hypersonic waveriders, AIAA-87-0272. AIAA 25th Aerospace Science Meeting, 1987.

[13] T. C. Rolim, P. G. d. P. Toro, M. A. S. Minucci, A. d. C. d. Oliveira, R. d. C. Follador, Experimental results of a mach 10 conical-flow derived waverider to 14-x hypersonic aerospace vehicle, Journal of Aerospace Technology and Management 3 (2011) 127–136.

[14] N. Hugo, V. Lago, Experimental analysis of waverider lift-to-drag ratio measurements in rarefied and supersonic regime (2021).

[15] H. Noubel, V. Lago, Correlation between waverider shock waves and aerodynamic forces in supersonic rarefied flow, experimental investigation in the wind tunnel marhy, Acta Astronautica (2022).

[16] G. S. Settles, Schlieren and shadowgraph techniques: visualizing phenomena in transparent media, Springer Science & Business Media, 2001.

[17] S. Coumar, Etude des mécanismes physiques induits pas un actionneur plasma appliqué au contrôle d'écoulements raréfiés super/hypersoniques dans le cadre de rentrées atmosphériques, Ph.D. thesis, Université d'Orléans (2017).

[18] R. Pattermann, F. Sturm, B. Döller, On stall behavior in aerobatic figures with an aerobatic glider, Technical Soaring 41 (2) 16–25.

[19] L. Kovacs, P.-Y. Passaggia, N. Mazellier, V. Lago, Detection method for shock-waves in viscous flows, Experiments in Fluids 63 (1) (2022) 1–16.

[20] M. Gaster, The structure and behaviour of laminar separation bubbles, Citeseer, 1967.